Origins of saccharide-dependent hydration at aluminate, silicate, and aluminosilicate surfaces

Benjamin J. Smith[a], Aditya Rawal[a], Gary P. Funkhouser[b], Lawrence R. Roberts[c], Vijay Gupta[d], Jacob N. Israelachvili[a,1], and Bradley F. Chmelka[a,1]

[a]Department of Chemical Engineering, University of California, Santa Barbara, CA 93106; [b]Halliburton, Duncan, OK 73536; [c]Roberts Consulting Group, 44 Windsor Avenue, Acton, MA 01720; and [d]RTI International, Research Triangle Park, NC 27709

Contributed by Jacob N. Israelachvili, March 25, 2011 (sent for review February 4, 2011)

Sugar molecules adsorbed at hydrated inorganic oxide surfaces occur ubiquitously in nature and in technologically important materials and processes, including marine biomineralization, cement hydration, corrosion inhibition, bioadhesion, and bone resorption. Among these examples, surprisingly diverse hydration behaviors are observed for oxides in the presence of saccharides with closely related compositions and structures. Glucose, sucrose, and maltodextrin, for example, exhibit significant differences in their adsorption selectivities and alkaline reaction properties on hydrating aluminate, silicate, and aluminosilicate surfaces that are shown to be due to the molecular architectures of the saccharides. Solid-state ^{1}H, ^{13}C, ^{29}Si, and ^{27}Al nuclear magnetic resonance (NMR) spectroscopy measurements, including at very high magnetic fields (19 T), distinguish and quantify the different molecular species, their chemical transformations, and their site-specific adsorption on different aluminate and silicate moieties. Two-dimensional NMR results establish nonselective adsorption of glucose degradation products containing carboxylic acids on both hydrated silicates and aluminates. In contrast, sucrose adsorbs intact at hydrated silicate sites and selectively at anhydrous, but not hydrated, aluminate moieties. Quantitative surface force measurements establish that sucrose adsorbs strongly as multilayers on hydrated aluminosilicate surfaces. The molecular structures and physicochemical properties of the saccharides and their degradation species correlate well with their adsorption behaviors. The results explain the dramatically different effects that small amounts of different types of sugars have on the rates at which aluminate, silicate, and aluminosilicate species hydrate, with important implications for diverse materials and applications.

Saccharide molecules and their interactions with inorganic oxide surfaces play crucial roles in a variety of natural and synthetic processes, including biomineralization, biomolecule synthesis, bone resorption, heterogeneous catalysis, corrosion inhibition, and cement hydration. For example, mono- and oligosaccharides are thought to control the morphologies and structures of carbonate skeletons in marine organisms through site-specific binding to the mineral phases (1, 2). Interactions of simple organic molecules with aluminosilicate surfaces and exchangeable cations in clays have been hypothesized to be key factors in abiotic syntheses of organic molecules (3). For example, sugar-silicate complexes have been shown to stabilize the abiotic formation of biologically important sugars, such as ribose (4). Similar interactions are thought to promote the adhesion of marine organisms at hydrated inorganic surfaces (5). Biofuels can be produced when polysaccharides are converted to monosaccharides and lower molecular weight alkenes at aluminosilicate zeolite surfaces by heterogeneous reactions in the presence of water (6). Saccharides have also been found to inhibit the corrosion of metal surfaces by forming thin adsorbed layers that prevent further oxidation (7). Finally, the hydration kinetics of aluminosilicate-based cements are critical to a number of modern technologies, notably as synthetic structural materials for large-scale construction projects and oil-well cementing, where saccharide additives are used to slow hydration processes and alter rheological properties (8).

Although saccharide-inorganic materials are ubiquitous in nature and used extensively in industry, saccharide interactions with heterogeneous hydrating inorganic oxides are not well understood at a molecular level. To a large extent, this has been due to challenges associated with the molecular characterization of the complicated multicomponent, multiphase, and nonequilibrium systems in which they occur. Interestingly, large variations in hydration behaviors of diverse oxides are observed in the presence of chemically similar saccharides, which we hypothesize are associated with subtle differences in their molecular interactions at specific solid surface sites. Here, we establish the molecular bases by which closely related saccharides bind to different oxide surfaces, identifying and correlating molecular interactions with specific structural features that influence macroscopic hydration properties. In particular, the structural transformations of glucose and sucrose and their interactions with silicate, aluminate, and aluminosilicate surfaces are analyzed to establish the molecular properties and processes that govern hydration of these technologically important materials.

Results and Discussion

Saccharide-Mediated Aluminate Hydration. The influences of different saccharides on the hydration of aluminates and silicates are due to their different stabilities in alkaline solutions and in their adsorption behaviors that depend on competitive interactions with water at specific surface sites. At a micron-scale, saccharides influence the morphological evolution of hydrating aluminate particles, such as tricalcium aluminate ($Ca_3Al_2O_6$, abbreviated as "C_3A" in cement chemistry). As shown in the scanning electron microscopy (SEM) images of Fig. 1, very different crystal morphologies are observed for the aluminate components following hydration for 4 h at 95 °C in the absence or presence of 1% glucose or sucrose, saccharides which have closely related molecular structures (Fig. 1). Initially, anhydrous C_3A (Fig. 1*A*) consists of crystalline particles ranging in size from 1–20 μm that rapidly hydrate in the presence of $CaSO_4 \cdot 2H_2O$ and without saccharides to form a mixture of aluminate hydration products, primarily as 1–10 μm acicular crystallites (Fig. 1*B*). Such needle-like crystal morphologies are consistent with the formation of ettringite ($Ca_6Al_2O_6(SO_4)_3 \cdot 32H_2O$) and calcium aluminate monosulfate ($Ca_4Al_2O_6(SO_4) \cdot 12H_2O$, referred to as "monosulfate"), both of which form hexagonal crystals that are the expected products of C_3A hydration with calcium sulfate dihydrate (9). By comparison, Fig. 1*C* shows an SEM image of C_3A

Author contributions: B.J.S., A.R., G.P.F., L.R.R., V.G., J.N.I., and B.F.C. designed research; B.J.S. and A.R. performed research; B.J.S., J.N.I., and B.F.C. analyzed data; and B.J.S., G.P.F., L.R.R., V.G., J.N.I., and B.F.C. wrote the paper.

The authors declare no conflict of interest.

[1]To whom correspondence should be addressed. E-mail: bradc@engineering.ucsb.edu and jacob@engineering.ucsb.edu.

This article contains supporting information online at www.pnas.org/lookup/suppl/doi:10.1073/pnas.1104526108/-/DCSupplemental.

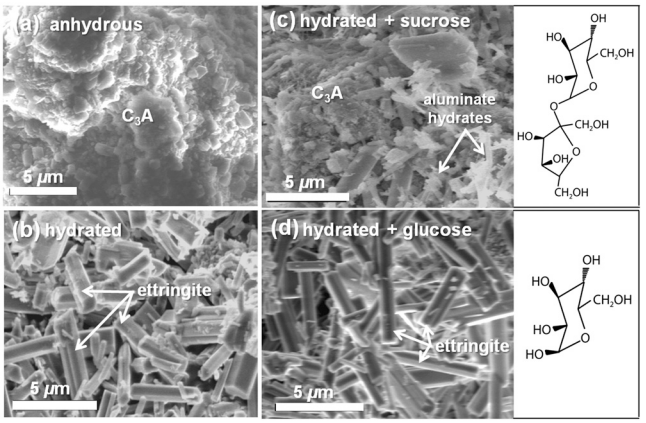

Fig. 1. Representative scanning electron micrographs of (*A*) anhydrous tricalcium aluminate and hydrated for 4 h at 95 °C with (*B*) no saccharide, (*C*) 1% sucrose, or (*D*) 1% glucose by weight of C_3A. The molecular structures of the saccharides are shown. Hydration occurs in the presence of $CaSO_4 \cdot 2H_2O$ to moderate the otherwise rapid hydration of tricalcium aluminate.

hydrated with 1% sucrose, which results in a notable decrease in the quantity of aluminate-hydrate crystals and with numerous anhydrous C_3A particles still present. Some acicular hydrates are observed, but the crystals are generally much fewer and smaller than those formed in the absence of saccharides (Fig. 1*B*). In contrast, the crystal morphologies of C_3A hydrated with 1% glucose (Fig. 1*D*) are very similar to those obtained without saccharides (Fig. 1*B*), indicating that glucose has much less influence than sucrose on the hydration of C_3A.

Quantitative analyses of tricalcium aluminate hydration. The extent of C_3A hydration and the quantities of different aluminate hydration products can be established in detail by solid-state 1D and 2D ^{27}Al NMR measurements. At very high magnetic fields (18.8 T), single-pulse 1D ^{27}Al magic angle spinning (MAS) NMR spectra of C_3A hydrated without and with saccharides (Fig. S1) show signals from $^{27}Al^{IV}$ moieties in anhydrous C_3A and $^{27}Al^{VI}$ species into which the $^{27}Al^{IV}$ moieties are converted during hydration. By comparing the relative integrated intensities of these signals, the extents of hydration can be estimated. In the absence of saccharides, 74% of anhydrous $^{27}Al^{IV}$ moieties in C_3A are converted into hydrated $^{27}Al^{VI}$ species (Table 1 and Fig. S1*A*). In combination, solid-state single-pulse ^{27}Al MAS and 2D $^{27}Al\{^1H\}$ heteronuclear correlation (HETCOR) NMR spectra (Fig. S2) allow different resolved $^{27}Al^{VI}$ species to be assigned and quantified in hydrated C_3A. The ^{27}Al peak assignments are based on previous studies (10, 11), and the 2D $^{27}Al\{^1H\}$ HETCOR measurements are consistent with the formation of six-coordinate $Al(OH)_6$ species, including ettringite (Fig. 2*A*), monosulfate, tricalcium aluminate hexahydrate ($Ca_3Al_2O_6 \cdot 6H_2O$), and dicalcium aluminate octahydrate ($Ca_2Al_2O_5 \cdot 8H_2O$). Without saccharides, ettringite (24%), monosulfate (19%), and $Ca_2Al_2O_5 \cdot 8H_2O$ (22%) are the dominant species, along with a minor fraction (9%) of $Ca_3Al_2O_6 \cdot 6H_2O$ (Table 1). These analyses allow the extents of hydration and relative quantities of aluminate hydration products to be compared with systems containing glucose, maltodextrin, and sucrose.

Notably, in the presence of small amounts of the different saccharides, the hydration of tricalcium aluminate is reduced by dramatically different extents under otherwise identical conditions. These differences are reflected in quantitative solid-state single-pulse ^{27}Al NMR analyses (Fig. S1*B–D*) of C_3A hydrated with 1% glucose, maltodextrin, or sucrose. As measured by the conversion of anhydrous $^{27}Al^{IV}$ to hydrated $^{27}Al^{VI}$ species (Table 1), sucrose most effectively inhibits overall C_3A hydration with only 28% conversion, followed by maltodextrin (53%) and glucose (60%). These results are consistent with the distinct product morphologies observed in Fig. 1, manifesting the significantly different influences that these saccharides have on C_3A hydration. The relative quantities of the different aluminate hydration products are estimated from single-pulse 1D ^{27}Al MAS spectra (Fig. S3) and are shown in Table 1. All of the saccharides examined inhibit the formation of monosulfate, whereas only sucrose delays the formation of all aluminate hydrates to significant extents. All aluminate hydrates form directly from the hydration of C_3A, whereas monosulfate can also form from the subsequent conversion of ettringite. This suggests that sucrose adsorbs onto C_3A surfaces, thereby passivating hydration sites and inhibiting the formation of other C_3A hydration products.

Saccharide–aluminate interactions. The different aluminate hydration behaviors in the presence of sucrose and glucose can be correlated to their significantly different adsorption properties on C_3A and its hydration products. Specific saccharide–aluminate interactions in hydrated C_3A can be probed by solid-state 2D $^{13}C\{^1H\}$ HETCOR NMR measurements that are sensitive to dipole–dipole couplings between ^{13}C and ^1H nuclei. For example, Fig. 3*A* shows the 2D $^{13}C\{^1H\}$ HETCOR spectrum acquired for C_3A hydrated in the presence of 1% ^{13}C-labeled glucose, in which correlated 2D signal intensity reveals interactions between ^{13}C and ^1H moieties that are in molecular proximity (<1 nm). Compared to the 1D single-pulse ^{13}C MAS NMR spectrum of crystalline glucose (Fig. 3*A*, *Top*), the absence of ^{13}C intensity correlations at 92 and 95 ppm from C1α and C1β moieties, along with the appearance of ^{13}C signals from carboxylate moieties ($-COO^-$, 185 ppm), alkyl groups ($-CH_2-$, 40 ppm; $-CH_3$, 20 ppm), and carbinol species (-CHOH, -COH, 55–85 ppm), establish that the cyclic form of glucose has completely degraded. Such signals are consistent with the formation of saccharinic or other short-chained carboxylic acids, which have previously been reported for glucose degradation in aqueous alkaline solutions (12).

Analysis of the intensity correlations in the 2D $^{13}C\{^1H\}$ HETCOR spectrum (Fig. 3*A*) of C_3A hydrated in the presence of glucose reveals specific interactions between glucose degradation species and aluminate hydration products. Strong intensity correlations are observed between the ^{13}C carbinol signal centered at 75 ppm and ^1H signals at 3.6 and 1.5 ppm (Fig. 3*A*, right red dashed box) associated with the carbinol protons and hydroxyl groups from aluminate ($^{27}Al^{VI}$) hydration products (Fig. S2),

Table 1. Relative populations of NMR-visible ^{27}Al species and overall conversion of Al^{IV} species in tricalcium aluminate to Al^{VI} products during hydration in the presence of saccharides

	Al^{IV}	Al^{VI}				
Saccharide	$Ca_3Al_2O_6$ (C_3A) 50–80 ppm, %	$Ca_3Al_2O_6 \cdot 6H_2O$ 11.0 ppm, %	ettringite 10.0 ppm, %	monosulfate 9.3 ppm, %	$Ca_2Al_2O_5 \cdot 8H_2O$ 8.6 ppm, %	% ^{27}Al conversion
none	26	9	24	19	22	74
1% glucose	40	12	19	6	23	60
1% maltodextrin	47	12	15	4	22	53
1% sucrose	72	6	8	4	10	28

From quantitative line-fitting of 1D ^{27}Al MAS NMR spectra in Figs. S1 and S3. Percent values are estimated to be accurate within ±2%.

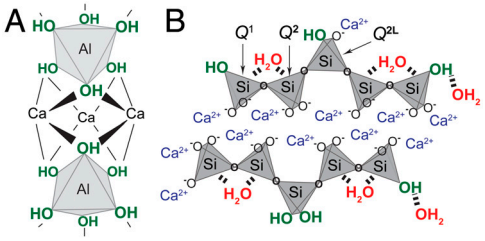

Fig. 2. Schematic diagrams of (*A*) hydroxylated Al^{VI} species in ettringite, and (*B*) the different four-coordinate Q^1, Q^2, and Q^{2L} silicate moieties in CSH.

respectively. This establishes that carbinol-containing glucose degradation products adsorb strongly on aluminate-hydrate surfaces, although the broadened ^{1}H signal does not allow interactions with specific hydrates to be distinguished. Intensity correlations observed between the ^{13}C signal at 185 ppm and ^{1}H protons at 1.5 ppm (Fig. 3*A*, left red dashed box) show additional molecular interactions between -COO^- moieties and aluminate-hydrate surfaces. Carboxylate groups in organic molecules likely bind to aluminate surfaces in aqueous environments through electrostatic interactions (Fig. 3*A*, *Inset i*), whereas carbinol moieties form hydrogen bonds (Fig. 3*A*, *Inset ii*). Intensity correlations between ^{13}C signals at 20 and 40 ppm associated with alkyl species and the ^{1}H signal at 1.5 ppm may result from intramolecular (i.e., directly bonded -CH_2- or -CH_3 protons) or intermolecular (i.e., -AlOH) interactions. Both types of interactions are expected to yield correlated signal intensity in similar regions of the 2D ^{13}C{^{1}H} HETCOR spectrum and are not resolved in Fig. 3*A*. Intramolecular interactions account for intensity correlations between ^{13}C signals at 185 and 40 ppm and the ^{1}H signal at 3.6 ppm associated with adjacent carbinol species. Using ^{13}C-labeled glucose, molecular interactions are thus observed between carboxylate and carbinol moieties found in glucose degradation products, providing direct evidence that these species adsorb onto, or are intercalated within, aluminate hydration products.

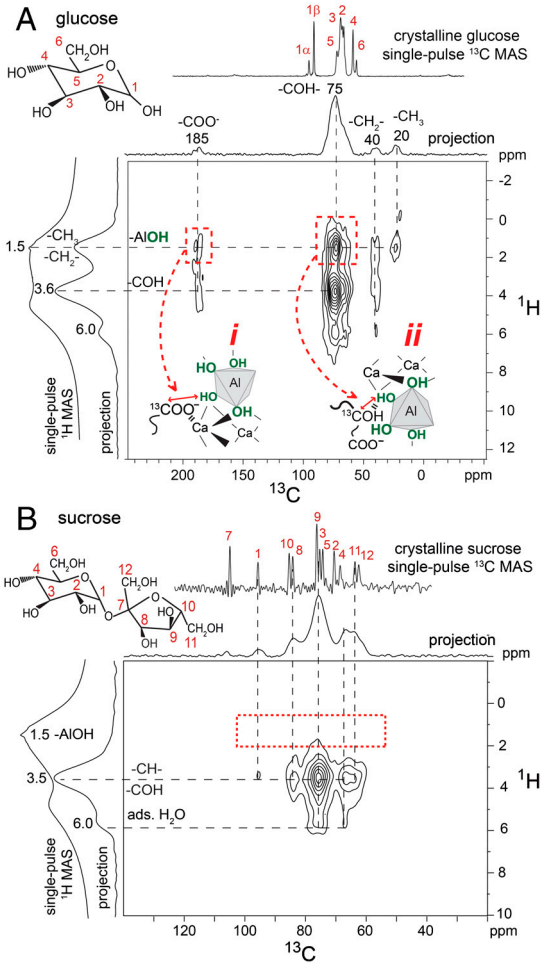

Fig. 3. Solid-state 2D ^{13}C{^{1}H} HETCOR NMR spectra acquired at 18.8 T, 298 K, 10 kHz MAS for hydrated tricalcium aluminate (4 h, 95 °C) in the presence of $CaSO_4 \cdot 2H_2O$ and with 1% (*A*) glucose or (*B*) sucrose by weight of C_3A. The *Insets* in (*A*) show glucose degradation moieties binding to aluminate surfaces through (*i*) -COO^- interactions and (*ii*) -COH hydrogen bonds.

In contrast, similar measurements under identical alkaline conditions show that sucrose does not degrade and does not adsorb on aluminate hydration products. Fig. 3*B* shows the solid-state 2D ^{13}C{^{1}H} HETCOR spectrum of hydrated C_3A in the presence of 1% ^{13}C-labeled sucrose that exhibits intensity correlations corresponding to dipole-dipole–coupled moieties associated with adsorbed sucrose molecules. All of the ^{13}C signals appear at similar chemical shifts, but are broadened, compared to those observed in the 1D single-pulse ^{13}C MAS NMR spectrum of crystalline sucrose (Fig. 3*B*, *Top*), consistent with intact adsorption of sucrose on C_3A. Intramolecular 2D intensity correlations are observed between multiple ^{13}C signals and ^{1}H signals centered at 3.6 ppm that also are present in the solid-state 2D ^{13}C{^{1}H} HETCOR spectrum of crystalline sucrose (Fig. S4). Importantly, no intensity correlations are observed between the ^{13}C signals and the ^{1}H signal centered at 1.5 ppm (Fig. 3*B*, red dashed box) that are associated with -AlOH moieties, indicating that the ^{13}C species are not in molecular proximity to aluminate-hydrate species. Unlike hydrating C_3A systems containing glucose, the 2D ^{13}C{^{1}H} intensity correlations establish that sucrose does not bind to aluminate-hydrate surfaces, the formation of which sucrose is notably most effective at inhibiting (Table 1).

Based on these results, we hypothesize that sucrose adsorbs intact selectively at C_3A surfaces, thereby inhibiting C_3A hydration. In contrast, the degradation species associated with glucose and maltodextrin adsorb nonselectively to aluminate hydration products, resulting in the delayed formation of monosulfate, as depicted schematically in Fig. 4. In alkaline solutions, the glucose ring structure opens at the carbon 1–5 oxygen linkage (Fig. 3*A*), to form a linear structure with a carboxyl endgroup, before degrading further (12). By comparison, sucrose is composed of glucose and fructose monomer units that are conjoined such that similar ring opening does not occur because the carbon 1–7 oxygen linkage prevents formation of a carboxyl moiety. This suggests that sucrose is a more effective hydration inhibitor because it selectively adsorbs at C_3A surfaces, with its ring structure intact, resulting in higher local surface coverages, compared to glucose or maltodextrin degradation species that also adsorb on diverse

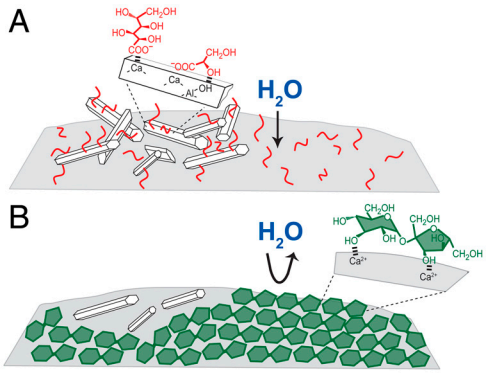

Fig. 4. Schematic diagrams depicting the different adsorption properties of (*A*) glucose degradation products (carboxylic acids, red) versus (*B*) sucrose (green) on tricalcium aluminate particles (gray) or aluminate hydration products, e.g., ettringite (white hexagons) under alkaline conditions. Whereas the glucose degradation species adsorb nonselectively, sucrose molecules are selective for the anhydrous aluminate moieties.

aluminate hydration products. The less-selective interactions of carboxylic acid species with aluminate hydration moieties are likely a consequence of their much higher dissociation constants (e.g., saccharinic acids, $pK_a < 4.0$ versus sucrose, $pK_a = 12.6$), which promote electrostatic interactions with cationic surface sites. The combination of 1D and 2D NMR techniques provides important insights on saccharide-dependent aluminate hydration and the molecular mechanisms that account for the distinctly different saccharide behaviors.

Saccharide-Mediated Silicate Hydration. ***Quantitative analyses of tricalcium silicate hydration.*** Similarly, the solution behaviors and/or structural transformations of saccharides under alkaline conditions also lead to different binding configurations and coverages at silicate surfaces that result in significantly different silicate hydration behaviors. As a technologically important example, the hydration of silicates such as tricalcium silicate (Ca_3SiO_5, often abbreviated as "C_3S"), are primarily responsible for setting and strength development of cements (9), which are often modified by saccharides that significantly affect bulk rheological or mechanical properties. The extent of C_3S hydration and formation of calcium-silicate-hydrate ("CSH," Fig. 2*B*) products are elucidated by quantitative single-pulse 1D ^{29}Si MAS NMR measurements, which show that certain saccharides more effectively suppress the formation of CSH during the early stages of hydration than others. For example, the single-pulse 1D ^{29}Si MAS spectra of C_3S hydrated for 4 h at 95 °C without and with saccharides (Fig. S5) show ^{29}Si signals from Q^0 species ("Q^n" refers to ^{29}Si atoms that are covalently bonded via bridging oxygen atoms to $n \leq 4$ other Si atoms) in anhydrous C_3S that are converted upon hydration to cross-linked Q^1, Q^{2L}, and Q^2 silicate species associated with CSH. Fig. 2*B* shows a postulated structure of CSH that is consistent with previous ^{29}Si NMR measurements (10), recent molecular modeling analyses (13, 14), small-angle neutron and X-ray scattering data (15, 16), and transmission electron microscopy studies (17). In the absence of saccharides, the extent of hydration can be established by comparing the relative integrated ^{29}Si NMR signal intensities from Q^0 (54%), Q^1 (22%), Q^{2L} (4%), and Q^2 (20%) ^{29}Si species, where hydration is measured as the conversion of anhydrous ^{29}Si Q^0 to hydrated Q^1, Q^{2L}, and Q^2 ^{29}Si species (Table 2 and Fig. S5*A*). Thus, under these conditions, approximately 46% of the ^{29}Si species have hydrated to form CSH. Similar analyses on C_3S under otherwise identical conditions, except containing 1% glucose, maltodextrin, or sucrose (Fig. S5 *B–D*), show that the conversion of ^{29}Si Q^0 species during hydration is reduced for all saccharides to 24, 8, and 3%, for glucose, maltodextrin, and sucrose, respectively. These measurements establish the significantly different influences of these saccharides on C_3S hydration, which follow the same sequence as observed for the aluminates, but with greater effect.

Saccharide–silicate interactions. The molecular origins of the different tricalcium silicate hydration properties in the presence of the saccharides are due to differences in their adsorption interactions at specific silicate surface sites. Two-dimensional NMR measurements resolve interactions between water, organic moieties, and silicate species that account for the suppression of cross-linked ^{29}Si species in hydrated C_3S. For example, molecular interactions between different silicate moieties and organic species are observed in the 2D ^{13}C{^{1}H} HETCOR spectrum of C_3S hydrated in the presence of 1% ^{13}C-labeled glucose (Fig. 5*A*). As with the aluminates, the absence of C1α and C1β ^{13}C signals at 92 and 95 ppm indicates that the cyclic form of glucose has completely degraded, with the appearance of ^{13}C signals at 182, 40, and 20 ppm being consistent with the formation of saccharinic or short-chained carboxylic acids. Intensity correlations are clearly observed between the carboxylate ^{13}C signals at 172 and 182 ppm and the ^{1}H signal at 1.3 ppm (Fig. 5*A*, left red dashed box) that is associated with the hydrated ^{29}Si Q^1 and Q^2 species (Fig. S6), along with the carbinol protons (3.6 ppm). Likewise, the carbinol ^{13}C signals centered at 75 ppm are correlated with the Q^1 and Q^2 silanol ^{1}H signals at 1.3 ppm (Fig. 5*A*, right red dashed box) and the carbinol ^{1}H signal at 3.6 ppm. These observations provide strong evidence that the glucose degradation products adsorb strongly on CSH surfaces and that both the -COO$^-$ and -COH moieties are in close proximities to the surface -SiOH species. Carboxylate groups are expected to bind to silicate surfaces in aqueous environments through electrostatic interactions (Fig. 5*A*, *Inset i*), with carbinol moieties adsorbing via hydrogen bonds

Table 2. Relative populations of ^{29}Si species and overall conversion of Q^0 species in tricalcium silicate to cross-linked Q^1, Q^{2L}, and Q^2 moieties during hydration in the presence of saccharides

Saccharide	Q^0, % > −76 ppm	Q^1, % −79 ppm	Q^{2L}, % −82 ppm	Q^2, % −85 ppm	% ^{29}Si conversion
none	54	22	4	20	46 (±3)
1% glucose	76	12	2	10	24 (±3)
1% maltodextrin	92	4	1	3	8 (±1)
1% sucrose	97	2	0	1	3 (±1)

From quantitative line-fitting of 1D ^{29}Si MAS NMR spectra in Fig. S5.

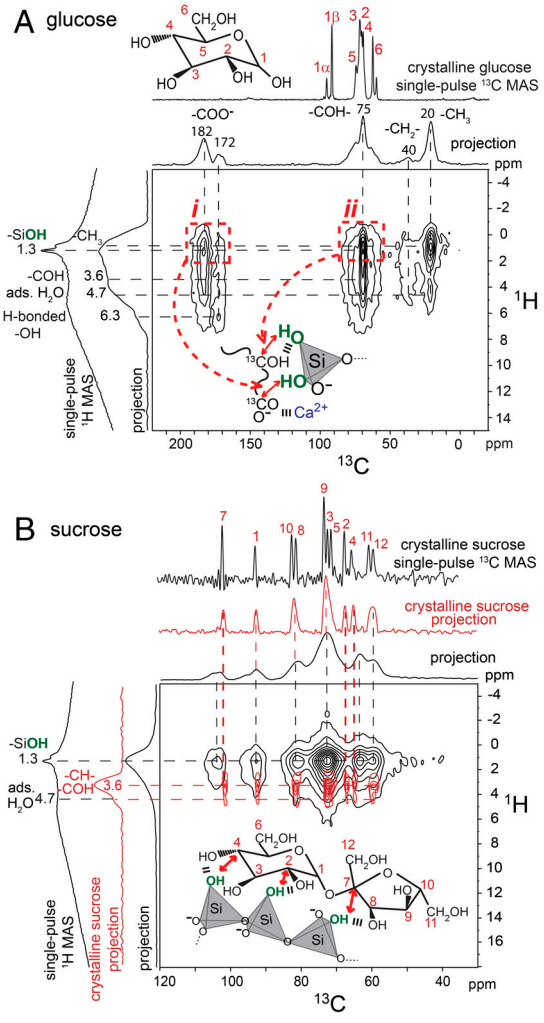

Fig. 5. Solid-state 2D ^{13}C{^{1}H} HETCOR NMR spectra acquired at 11.7 T, 298 K, 10 kHz MAS for hydrated tricalcium silicate (4 h, 95 °C) with 1% (*A*) glucose or (*B*) sucrose by weight of C_3S. The *Insets* in (*A*) show glucose degradation moieties binding to CSH surfaces through (*i*) -COO$^-$ interactions and (*ii*) -COH hydrogen bonds. The *Inset* in (*B*) shows sucrose binding to CSH surfaces through hydrogen bonds.

(Fig. 5*A*, *Inset ii*). Weaker intensity correlations observed between the ^{13}C signals at 172, 182, and 75 ppm and the ^{1}H signal at 4.7 ppm indicate coadsorbed water in close proximity to the -COO^- and -COH moieties. Weak intensity correlations between these ^{13}C signals and the ^{1}H signal at 6.3 ppm result from nearby hydrogen-bonded -OH moieties. Intramolecular interactions account for the correlated intensity between ^{13}C signals at 20 ppm and the ^{1}H signal at 0.9 ppm associated with alkyl species (i.e., -CH_3, -CH_2-). The molecular interactions between CSH moieties and both -COH and -COO^- groups establish that adsorbed glucose degradation products, as opposed to glucose itself, are responsible for inhibiting C_3S hydration.

Similar 2D NMR analyses of C_3S hydrated in the presence of sucrose manifest site-specific interactions between sucrose and silicate hydration products. Fig. 5*B* shows 2D $^{13}C\{^{1}H\}$ HETCOR spectra of crystalline sucrose (red) and C_3S hydrated with 1% ^{13}C-labeled sucrose (black), which are superimposed to emphasize similarities and differences in their correlated signals. Comparison of the ^{13}C signals in the 1D projections of crystalline sucrose and hydrated C_3S establish that sucrose molecules adsorb intact with no degradation products observed (within the sensitivity limits of the measurements). Furthermore, strong intensity correlations are observed between all sucrose ^{13}C signals and the ^{1}H signal at 1.3 ppm (Fig. 5*B*, black) associated with the hydrated Q^1 and Q^2 silanol species. This indicates that sucrose molecules are adsorbed strongly at CSH surface sites in configurations where all of the carbon atoms can be in close (<1 nm) proximity to the hydrate surfaces. Intramolecular intensity correlations are observed between multiple ^{13}C signals and the ^{1}H signal centered at 3.6 ppm, which are also observed in the solid-state 2D $^{13}C\{^{1}H\}$ HETCOR spectrum of crystalline sucrose (Fig. 5*B*, red). Weaker intensity correlations observed between the ^{13}C signals at 67 and 75 ppm and the ^{1}H signal at 4.7 ppm indicate that some coadsorbed water is also in close proximity to the sucrose molecules. However, compared to the 2D $^{13}C\{^{1}H\}$ HETCOR spectrum of C_3S hydrated with 1% glucose (Fig. 5*A*), these intensity correlations with water are significantly weaker, establishing that sucrose more effectively excludes water from CSH surface sites.

Additionally, comparison of the ^{13}C chemical shifts between crystalline sucrose (Fig. 5*B*, red) and sucrose adsorbed on CSH (Fig. 5*B*, black) allow specific ^{13}C moieties that interact most strongly with the hydrated silicate species to be identified. When an organic molecule binds to an inorganic ion or surface, the local ^{13}C electronic environments can be altered, leading to changes in the ^{13}C isotropic chemical shifts. For example, the isotropic ^{13}C chemical shifts of carbon atoms 7, 2, and 4 are each displaced by 2–3 ppm for the adsorbed species, compared to crystalline sucrose, whereas all other ^{13}C shifts are nearly the same ($|\Delta\delta| < 1$ ppm). Importantly, this suggests that sucrose molecules interact via several carbon moieties with multiple CSH surface sites (Fig. 5*B*, *Inset*) leading to stronger adsorption. Multiple interaction sites are expected similarly to promote sucrose adsorption on C_3S where -SiOH moieties are present under aqueous conditions, though in relatively low fractions that are challenging to observe. These measurements establish that, compared to glucose, sucrose more effectively inhibits C_3S hydration, because of the presence of multiple interaction sites on (nondegraded) disaccharide molecules, which lead to strong sucrose adsorption that competitively excludes water at CSH sites.

Saccharide–Aluminosilicate Interaction Forces. The different molecular interactions of saccharides at aluminate and silicate surfaces observed by 2D NMR similarly result in distinct adsorption and hydration behaviors at aluminosilicate surfaces. Surface forces measurements, employing molecularly smooth aluminosilicate mica sheets, corroborate the molecular (<1 nm) NMR analyses and quantify longer-range (1–100 nm) forces between aluminosilicate surfaces hydrated in the presence of the different saccharides and/or their degradation products. For example, Fig. 6 shows normal forces measured as functions of the distance separating two aluminosilicate surfaces immersed in otherwise identical alkaline solutions (pH 12.7, 25 °C) initially containing none or 0.2 wt%, of the different saccharides. In the absence of saccharides, the forces between the aluminosilicate surfaces are consistent with Derjaguin–Landau–Verwey–Overbeek (DLVO) theory (18), which describes the combination of attractive van der Waals and repulsive electric double-layer forces that exist between two surfaces in aqueous solutions. The characteristic decay length of the interaction, or Debye length ($1/\kappa$), measured to be 1.5 nm (Fig. 6, *Inset*), is close to the value of 1.1 nm calculated from DLVO theory (19). A so-called "hard wall," where the repulsive force increases rapidly at very short separation distances, is observed at approximately 1 nm, due to "steric-hydration" forces caused by water and cations solvated at the mica surfaces. The surface forces apparatus (SFA) measurements permit quantitative comparisons to be made among different alkaline solutions, including those containing saccharides that may be adsorbed onto the hydrated aluminosilicate mica surfaces.

Similar surface force measurements between mica surfaces in contact with alkaline solutions containing 0.2 wt% glucose or sucrose establish very different behaviors for the different saccharides. As for the alkaline solution alone, the force-distance profiles for glucose and sucrose (Fig. 6) exhibit similar hard walls, though at significantly different separation distances of approximately 1 nm for glucose and 7 nm for sucrose. For glucose, the hard wall at 1 nm is the same as that observed in the aqueous solution without saccharides, indicating that most of the organic species have been removed from the mica. The hard-wall repulsion at 1 nm provides quantitative evidence that the alkaline glucose degradation products adsorb relatively weakly on the aluminosilicate mica surfaces and can be "squeezed out" by fluid convection as the mica surfaces approach molecular contact.

In contrast, for sucrose the 7-nm hard wall is significantly larger than observed for glucose or the alkaline solution alone. This is due to steric forces between strongly adsorbed multilayers of sucrose molecules on the mica surfaces, which remain bound as the surfaces are brought together, thereby presenting an addi-

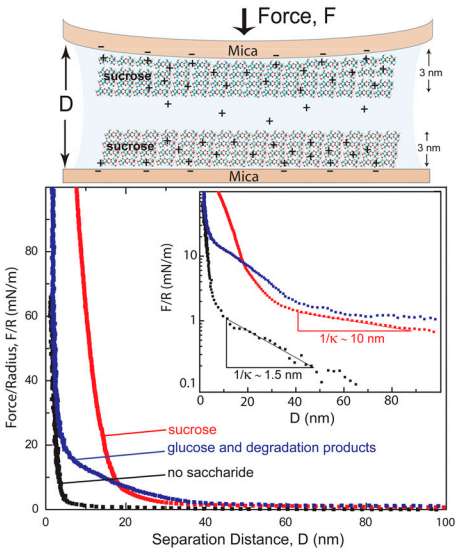

Fig. 6. Representative repulsive force-distance profiles, $F(D)$, measured normal on approach of two aluminosilicate mica surfaces immersed in otherwise identical 75 mM NaOH solutions (pH 12.7, 25 °C), but initially containing no saccharide, 0.2 wt% glucose, or 0.2 wt% sucrose. The *Inset* shows the same data on a semilog scale for comparison with the exponential behavior expected for a repulsive electrostatic "double layer" (DLVO theory). A schematic diagram of adsorbed sucrose multilayers at small mica surface separations is shown above.

tional strong repulsive contribution. The binding of sucrose on silicates established by solid-state NMR (Fig. 5*B*) suggests that the sucrose molecules adsorb in a planar fashion on the mica surfaces. This is similar to the stacking configuration of sucrose molecules in its monoclinic crystal, which are separated by approximately 0.8 nm (20). The 7-nm hard wall corresponds to multiple layers (approximately 4–5) of strongly adsorbed sucrose molecules on each mica surface (Fig. 6, *Top*), which remain intact even at relatively high local pressures (≥10 atm). This establishes that sucrose forms multilayers on the aluminosilicate surfaces, possibly through complexation with cations near the negatively charged mica or by precipitation from the aqueous solution.

Quantitative analyses of the force-distance profiles for glucose and sucrose indicate that complexation with cations occurs near the aluminosilicate surface and confirms strong sucrose adsorption at the mica surfaces. Comparison of the force-distance curves for glucose and sucrose (Fig. 6, *Inset*) reveals repulsive interactions with significantly different decay lengths as the mica surfaces approach, which reflect their different adsorption properties on hydrated aluminosilicate mica, as similarly observed and discussed for the aluminates and silicates above. Longer-range interactions observed at separation distances of about 40–100 nm are due to electrostatic interactions associated with the double layers near the surfaces of organic species adsorbed on the mica. The Debye lengths ($1/\kappa$), determined directly from the slopes of the linefits in this region (Fig. 6, *Inset*), are approximately 10 nm in the presence of sucrose or glucose. The longer Debye lengths, in comparison to alkaline solutions without saccharide ($1/\kappa \sim 1.5$ nm), are consistent with cation-saccharide complexation near the anionic mica surfaces, which is expected to result in decreased overall concentrations of cations in the bulk solutions (e.g., $\kappa \propto [Na^+_{bulk}]^{1/2}$). The SFA results establish that sucrose adsorbs more strongly than glucose (or the latter's associated degradation products) and in multilayers (for a sufficiently high concentration) on the aluminosilicate mica surfaces in aqueous alkaline media. Such strong adsorption appears to be enhanced by cation complexation and the multiple interaction sites established by the molecular-level NMR analyses.

Conclusions

The very different hydration behaviors of aluminates, silicates, and aluminosilicates in the presence of the closely related saccharides glucose, sucrose, and maltodextrin are shown to be due to their different alkaline stabilities, adsorption selectivities at oxide surfaces, and binding strengths. Such different hydration and adsorption properties are shown to be directly related to subtle but important differences in the molecular structures of the saccharides. Solid-state NMR spectroscopy and surface forces measurements establish over complementary length scales (<1 nm and 1–100 nm, respectively) the transformations and interactions of the respective mono- and disaccharide species at silicate, aluminate, and aluminosilicate surfaces. Two-dimensional $^{13}C\{^1H\}$ HETCOR NMR spectra of hydrated tricalcium aluminate and silicate establish that glucose degradation species interact nonselectively with aluminate and silicate hydration products and suggest selective adsorption of sucrose at C_3A surface sites and multiple interactions with silicate hydrates. Quantitative surface force measurements furthermore establish the formation of strongly adsorbed sucrose multilayers on hydrated aluminosilicate surfaces that are stable at relatively high local pressures, compared to weak binding of glucose degradation species.

The advanced NMR and surface force techniques demonstrated here are applicable generally to other systems where organic species interact at heterogeneous aluminate, silicate, or aluminosilicate surfaces. Such measurements can be used to establish molecular criteria for the design or selection of saccharide species that mediate surface reactions, such as hydration, corrosion, or adhesion. The resulting insights are expected to contribute directly and broadly toward understanding the molecular-level interactions between saccharides and similar hydrating oxide surfaces, which occur in cements, biominerals, abiotic syntheses of organic molecules, heterogeneous catalysis of sugars, and corrosion inhibition.

Materials and Methods

Tricalcium aluminate ($Ca_3Al_2O_6$, CTLGroup), tricalcium silicate (Ca_3SiO_5, CTLGroup), and calcium sulfate dihydrate (gypsum, $CaSO_4 \cdot 2H_2O$, Sigma-Aldrich) were used as received. D-glucose and sucrose, including 99% ^{13}C-enriched species, were obtained from Sigma-Aldrich and used as received. Maltodextrin (Main Street Ingredients) had a dextrose equivalent of 40. Hydrated materials were prepared by mixing the anhydrous materials and saccharide species with water in a high shear blender (Fisher Scientific) at 10,000 rpm for 1 min. The resulting mixtures were measured to be highly alkaline, with pH values of 12.7 (±0.1). Water-to-solids mass ratios of 0.50 and 2.00 were used for systems containing C_3S, and C_3A, respectively. For the cases where saccharides were present, they were added in concentrations of 1.0% by weight of C_3S or C_3A. All C_3A samples were hydrated with calcium sulfate dihydrate present in quantities of 50% by weight of C_3A; all C_3S samples were hydrated without gypsum. After mixing, all materials were poured into polyethylene containers and hydrated for 4 h at 95 °C and 100% relative humidity. Following hydration, the products were ground into a powder, immersed in liquid N_2, and evacuated at 0.10 Torr and 233 K to remove unreacted water and quench the hydration process (10). All NMR spectroscopy, SFA, and SEM experimental details are provided in *SI Text*.

ACKNOWLEDGMENTS. The authors thank C. Edwards, R. Prud'homme, and B. Figura for helpful discussions. This work was supported by a grant from Halliburton, Inc. The measurements were conducted using the Central Facilities of the University of California, Santa Barbara Materials Research Laboratory supported by the Materials Research Science and Engineering Centers program of the US National Science Foundation (Award DMR-05-20415).

1. Wang DB, Wallace AF, De Yoreo JJ, Dove PM (2009) Carboxylated molecules regulate magnesium content of amorphous calcium carbonates during calcification. *Proc Natl Acad Sci USA* 106:21511–21516.
2. Gertman R, Ben Shir I, Kababya S, Schmidt A (2008) In situ observation of the internal structure and composition of biomineralized *Emiliania huxleyi* calcite by solid-state NMR spectroscopy. *J Am Chem Soc* 130:13425–13432.
3. Smith JV (1998) Biochemical evolution. I. Polymerization on internal, organophilic silica surfaces of dealuminated zeolites and feldspars. *Proc Natl Acad Sci USA* 95:3370–3375.
4. Lambert JB, Gurusamy-Thangavelu SA, Ma KBA (2010) The silicate-mediated formose reaction: Bottom-up synthesis of sugar silicates. *Science* 327:984–986.
5. Zeng HB, Hwang DS, Israelachvili JN, Waite JH (2010) Strong reversible Fe^{3+}-mediated bridging between dopa-containing protein films in water. *Proc Natl Acad Sci USA* 107:12850–12853.
6. Chheda JN, Huber GW, Dumesic JA (2007) Liquid-phase catalytic processing of biomass-derived oxygenated hydrocarbons to fuels and chemicals. *Angew Chem Int Ed Engl* 46:7164–7183.
7. Raja PB, Sethuraman MG (2008) Natural products as corrosion inhibitor for metals in corrosive media. *Mater Lett* 62:113–116.
8. Zhang J, Weissinger EA, Peethamparan S, Scherer GW (2010) Early hydration and setting of oil well cement. *Cem Concr Res* 40:1023–1033.
9. Taylor HFW (1990) *Cement Chemistry* (Academic, London).
10. Rawal A, et al. (2010) Molecular silicate and aluminate species in anhydrous and hydrated cements. *J Am Chem Soc* 132:321–7337.
11. Skibsted J, Henderson E, Jakobsen HJ (1993) Characterization of calcium aluminate phases in cements by ^{27}Al MAS NMR spectroscopy. *Inorg Chem* 32:1013–1027.
12. Yang BY, Montgomery R (1996) Alkaline degradation of glucose. *Carbohydr Res* 280:27–45.
13. Richardson IG (2008) The calcium silicate hydrates. *Cem Concr Res* 38:137–158.
14. Pellenq RJM, et al. (2009) A realistic molecular model of cement hydrates. *Proc Natl Acad Sci USA* 106:16102–16107.
15. Allen AJ, Thomas JJ, Jennings HM (2007) Composition and density of nanoscale calcium-silicate-hydrate in cement. *Nat Mater* 6:311–316.
16. Skinner LB, Chae SR, Benmore CJ, Wenk HR, Monteiro PJM (2010) Nanostructure of calcium silicate hydrates in cements. *Phys Rev Lett* 104:195502.
17. Xu Z, Viehland D (1996) Observation of a mesostructure in calcium silicate hydrate gels of portland cement. *Phys Rev Lett* 77:952–955.
18. Verwey EJW, Overbeek JTG (1948) *Theory of Stability of Lyophobic Colloids* (Elsevier, Amsterdam).
19. Israelachvili JN (1992) *Intermolecular and Surface Forces,* (Elsevier, London), Vol 2.
20. Beevers CA, Mcdonald TRR, Robertson JH, Sterns F (1952) The crystal structure of sucrose. *Acta Crystallogr* 5:689–690.